"snow line" at a few AU and volatile-rich c outside. It will be interesting to see whether the usual migration mechanism that is invoked to alter planetary orbits—tidal interactions with the gaseous protoplanetary disk—could draw together two planets from such different regions of the disk. Or whether the compositions and densities of the planets could have changed with time, for example, because of the preferential erosion of the smaller planet's atmosphere by stellar irradiation (*16*) (fig. S21). Perhaps a combination of these factors will ultimately explain this puzzling pair of planets.

References and Notes

1. M. Mayor, D. Queloz, *Nature* **378**, 355 (1995).
2. D. N. C. Lin, P. Bodenheimer, D. C. Richardson, *Nature* **380**, 606 (1996).
3. W. J. Borucki *et al*., *Science* **327**, 977 (2010); 10.1126/science.1185402.
4. D. G. Koch *et al*., *Astrophys. J.* **713**, L79 (2010).
5. D. A. Caldwell *et al*., *Astrophys. J.* **713**, L92 (2010).
6. J. M. Jenkins *et al*., *Proc. SPIE* **7740**, 7740-0D (2010).
7. J. M. Jenkins *et al*., *Astrophys. J.* **713**, L87 (2010).
8. A. V. Kel'manov, B. Jeon, *IEEE Trans. Signal Process.* **52**, 645 (2004).
9. E. B. Ford *et al*. (2012); http://arxiv.org/abs/1201.5409.
10. J. H. Steffen *et al*., *Mon. Not. R. Astron. Soc.* **421**, 2342 (2012).
11. D. C. Fabrycky *et al*., (2012); http://arxiv.org/abs/1201.5415.
12. C. Marchal, G. Bozis, *Celestial Mech.* **26**, 311 (1982).
13. B. Gladman, *Icarus* **106**, 247 (1993).
14. R. Barnes, R. Greenberg, *Astrophys. J.* **647**, L163 (2006).
15. W. J. Chaplin *et al*., *Science* **332**, 213 (2011).
16. See supplementary materials available on *Science* Online.
17. J. A. Carter *et al*., *Science* **331**, 562 (2011); 10.1126/science.1201274.
18. K. Mandel, E. Agol, *Astrophys. J.* **580**, L171 (2002).
19. C. J. F. ter Braak, J. A. Vrugt, *Stat. Comput.* **16**, 239 (2006).
20. R. A. Marcus, S. T. Stewart, D. Sasselov, L. Hernquist, *Astrophys. J.* **700**, L118 (2009).
21. J. Miralda-Escudé, *Astrophys. J.* **564**, 1019 (2002).
22. J. J. Lissauer *et al*., *Nature* **470**, 53 (2011).
23. W. D. Cochran *et al*., *Astrophys. J. Suppl. Ser.* **197**, 7 (2011).
24. T. N. Gautier *et al*., *Astrophys. J.* **749**, 15 (2012).
25. D. Charbonneau *et al*., *Nature* **462**, 891 (2009).
26. A. P. Hatzes *et al*., *Astrophys. J.* **743**, 75 (2011).
27. N. M. Batalha *et al*., *Astrophys. J.* **729**, 27 (2011).
28. J. N. Winn *et al*., *Astrophys. J.* **737**, L18 (2011).
29. J. J. Fortney, M. S. Marley, J. W. Barnes, *Astrophys. J.* **659**, 1661 (2007).

Acknowledgments: NASA's Science Mission Directorate provided funding for the Kepler Discovery mission. J.A.C. and D.C.F. acknowledge support by NASA through Hubble Fellowship grants HF-51267.01-A and HF-51272.01-A awarded by the Space Telescope Science Institute, which is operated by the Association of Universities for Research in Astronomy, Incorporated, for NASA, under contract NAS 5-26555. E.A. acknowledges NSF Career grant AST-0645416 and thanks the Center for Astrophysics, where this work began. W.J.C., A.M., and Y.E. acknowledge the financial support of the UK Science and Technology Facilities Council (STFC). Funding for the Stellar Astrophysics Centre (SAC) is provided by the Danish National Research Foundation. The research is supported by the ASTERISK project (ASTERoseismic Investigations with SONG and Kepler) funded by the European Research Council (grant agreement no. 267864). S.H. acknowledges financial support from the Netherlands Organization for Scientific Research (NWO). Computational time on Kraken at the National Institute of Computational Sciences was provided through NSF TeraGrid allocation TG-AST090107. J.N.W. was supported by the NASA Kepler Participating Scientist program through grant NNX12AC76G. Refer to the supplementary materials for access information to data used in this work.

Supplementary Materials

www.sciencemag.org/cgi/content/full/science.1223269/DC1
Materials and Methods
Supplementary Text
Figs. S1 to S21
Tables S1 to S9
References (*30*–*98*)
Movie S1

12 April 2012; accepted 11 June 2012
Published online 21 June 2012;
10.1126/science.1223269

Non-Centrosymmetric Cylindrical Micelles by Unidirectional Growth

Paul A. Rupar,[1] Laurent Chabanne,[1] Mitchell A. Winnik,[2]* Ian Manners[1]*

Although solution self-assembly of block copolymers (BCPs) represents one of the most promising approaches to the creation of nanoparticles from soft matter, the formation of non-centrosymmetric nanostructures with shape anisotropy remains a major challenge. Through a combination of crystallization-driven self-assembly of crystalline-coil BCPs in solution and selective micelle corona cross-linking, we have created short (about 130 nanometers), monodisperse cylindrical seed micelles that grow unidirectionally. These nanostructures grow to form long, non-centrosymmetric cylindrical A-B and A-B-C block co-micelles upon the addition of further BCPs. We also illustrate the formation of amphiphilic cylindrical A-B-C block co-micelles, which spontaneously self-assemble into hierarchical star-shaped supermicelle architectures with a diameter of about 3 micrometers. The method described enables the rational creation of non-centrosymmetric, high aspect ratio, colloidally stable core-shell nanoparticles in a manner that until now has been restricted to the biological domain.

The bottom-up fabrication of devices and functional structures using nanoparticles as building blocks is a primary objective within the field of nanotechnology. As a consequence, improving the control of particle shape and composition in the nanoscopic size regime remains an important challenge (*1*). Although difficult to create, especially from soft materials, non-centrosymmetric structures are especially attractive because they can possess complex interparticle interactions useful for the bottom-up design of hierarchical assemblies (*2*, *3*). This is commonly illustrated in many biological systems: For example, non-centrosymmetric α-β heterodimer tubulin proteins aggregate head to tail to form polar microtubules, hierarchical architectures where asymmetry is critical for their cellular functions (*4*).

The solution self-assembly of block copolymers (BCPs) has emerged as a versatile technique to generate core-shell nanoparticles of controllable shape, size, and function. When placed in a block-selective solvent, BCPs assemble into a variety of different morphologies that are influenced by polymer molecular weights and block ratios, with further control possible through the manipulation of environmental conditions such as temperature, solvent, and concentration (*5*–*9*). Although progress has been achieved in BCP self-assembly, examples of the successful formation of nanoparticles with shape anisotropy and low symmetry are rare. Few approaches are available to prepare block copolymer–based nanoparticles, which are non-centrosymmetric (*10*). These are characterized by a relatively limited range of morphologies, sizes, and composition control, and few examples of nonspherical nanostructures have been described. The use of linear triblock copolymers to form non-centrosymmetric nanocylinders (*11*, *12*) and nanodiscs (*13*, *14*) after block-selective cross-linking in the bulk state has been reported. In an alternative approach, non-centrosymmetric nanoparticles have been formed in solutions containing two different diblock copolymers where the opposite sides of the structures express only one of the diblock copolymers (*15*–*17*). Giant amphiphilic diblock copolymer brushes have also been created by sequential ring-opening metathesis polymerization of macromonomers (*18*).

A recent development in the field of BCP fabrication involves the discovery of a process termed crystallization-driven self-assembly (CDSA) (*19*). CDSA occurs when crystalline-coil BCP unimers (molecularly dissolved BCPs) are placed in a solvent selective for the coil block (Fig. 1A). Under these conditions, the crystallization of the core-forming polymer block directs the formation of low-curvature structures such as cylinders and platelet micelles (*20*). In several cases, CDSA has been demonstrated to be a living process because the ends or edges of the micelles remain active to the addition of further unimer (*19*, *20*). Elongation via epitaxial growth is observed

[1]School of Chemistry, University of Bristol, Bristol BS8 1TS, UK. [2]Department of Chemistry, University of Toronto, Toronto, Ontario M5S 3H6, Canada.

*To whom correspondence should be addressed. E-mail: mwinnik@chem.utoronto.ca (M.A.W.); ian.manners@bristol.ac.uk (I.M.)

provided that there is a sufficient lattice match between the existing crystalline core and that formed by the added unimer (Fig. 1A) (*20*). Furthermore, cylindrical micelles of well-defined and controllable contour length and with narrow length distributions are readily accessible when unimers are added to colloidal dispersions of short, preformed cylindrical seed micelles (*21*). In recent years, CDSA processes have been used to access elongated structures for a range of crystalline-coil BCPs, including those containing poly(ferrocenyldimethylsilane) (PFS) (*19*), poly(ferrocenyldimethylgermane) (*20*), poly(3-hexylthiophene) (*22*, *23*), polylactide (*24*), polyethylene (*25*), polyacrylonitrile (*26*), and poly(ε-caprolactone) (*27*) crystalline core–forming blocks. Recently, hexaperihexabenzocoronenes, a class of aromatic small molecules, have been shown to form segmented semiconducting nanotubes in a process analogous to CDSA (*28*).

Although CDSA is emerging as a promising, versatile tool with which to create rationally designed micelles of well-defined size, shape, and spatially controlled composition, this method has been limited to the creation of centrosymmetric nanostructures. This symmetry constraint arises because epitaxial growth occurs bidirectionally off the opposing ends of a crystallized micelle core (Fig. 1A) (*19*). To obtain unidirectional growth, we required a method to create cylindrical seeds where one exposed end is effectively blocked to further elongation. To access such structures, we envisioned an approach whereby, in a first step, the ends of a cylindrical B-A-B triblock co-micelle would be blocked by coronal cross-linking (*29*) to prevent the ends from initiating CDSA (Fig. 1B). In a second step, we conceived that the central micelle block could be selectively dissolved to leave two short daughter micelles, each with a single blocked end and a newly exposed, active crystalline core at the opposite terminus (Fig. 1B). Because only one of the exposed daughter micelle core ends would be expected to participate in CDSA, these new, short, cylindrical seeds should only grow in a single direction and would thereby provide a platform for the creation of non-centrosymmetric cylinders.

To explore the feasibility of this end-blocking approach, we performed studies on cylinders derived from (PI-*b*-PFS) (PI is polyisoprene). We previously established coronal cross-linking of PI in such BCP micelles as a means to achieve permanent micelle stability in good solvents for both blocks (*30*, *31*). We used a diblock copolymer, PI_{1424}-*b*-PFS_{63} (table S1), with a very long corona-forming PI block because we reasoned that, in solution, the corona chains would partially cover the high-energy PFS crystalline core faces of the micelles to minimize exposure to the selective solvent. Thus, we predicted that cross-linking of the corona chains should immobilize the PI chains, thereby rendering the core face inaccessible and efficiently inhibiting CDSA (Fig. 1B). To test this hypothesis, we created a decane colloidal dispersion of cylindrical M(PI_{1424}-*b*-PFS_{63}) micelles (the prefix "M" denotes that the block copolymer is incorporated into a micelle) with an average contour length of 121 nm and a narrow length distribution [polydispersity index (PDI) = 1.05] (Fig. 2A and figs. S1 and S2) (*32*). Karstedt's catalyst–promoted hydrosilylation with tetramethyldisiloxane was then used to cross-link the PI corona of the micelles to generate ^{XL}M(PI_{1424}-*b*-PFS_{63}) cylinders (Fig. 2B; superscript XL implies cross-linked) (*30*). Next, we added a tetrahydrofuran (THF) solution of PFS_{60}-*b*-$PDMS_{660}$ [PDMS is poly(dimethylsiloxane)] (table S1) unimers to separate samples of the non–cross-linked M(PI_{1424}-*b*-PFS_{63}) and the cross-linked ^{XL}M(PI_{1424}-*b*-PFS_{63}) micelles. As anticipated, when PFS_{60}-*b*-$PDMS_{660}$ unimers were added to preformed non–cross-linked M(PI_{1424}-*b*-PFS_{63}) micelles as a control, the PFS_{60}-*b*-$PDMS_{660}$ unimers were incorporated at the cylinder ends, which resulted in the formation of M(PFS_{60}-*b*-$PDMS_{660}$)-*b*-M(PI_{1424}-*b*-PFS_{63})-*b*-M(PFS_{60}-*b*-$PDMS_{660}$) triblock co-micelles with an increased average contour length of 275 nm (PDI = 1.16) (Fig. 2C and fig. S3). However, in the case of the cross-linked ^{XL}M(PI_{1424}-*b*-PFS_{63}) micelles, the vast majority of the micelles (98%) did not elongate; instead, several micrometer-long self-nucleated M(PFS_{60}-*b*-$PDMS_{660}$) homomicelles were detected in addition to the unchanged cross-linked ^{XL}M(PI_{1424}-*b*-PFS_{63}) micelles (Fig. 2D and fig. S4). We therefore concluded that the corona cross-linking strategy provides an efficient method of blocking micelle termini toward further participation in CDSA.

With confidence in our ability to inhibit CDSA, we began the creation of a sample of triblock co-micelles with two cross-linkable corona domains located on the end blocks and a non–cross-linkable corona domain as the central block. PI_{1424}-*b*-PFS_{63} unimers were added to preformed cylindrical M(PFS_{60}-*b*-$PDMS_{660}$) micelles to give B-A-B cylindrical M(PI_{1424}-*b*-PFS_{63})-*b*-M(PFS_{60}-*b*-$PDMS_{660}$)-*b*-M(PI_{1424}-*b*-PFS_{63}) triblock co-micelles with a length of 430 nm (PDI = 1.02) (figs. S5 to S7). The PI corona was cross-linked (Fig. 3, A and B), and then further PFS_{60}-*b*-$PDMS_{660}$ unimers were added to the cross-linked ^{XL}M(PI_{1424}-*b*-PFS_{63})-*b*-M(PFS_{60}-*b*-$PDMS_{660}$)-*b*-^{XL}M(PI_{1424}-*b*-PFS_{63}) triblock co-micelles. As desired, almost all (98%) of the ^{XL}M(PI_{1424}-*b*-PFS_{63})-*b*-M(PFS_{60}-*b*-$PDMS_{660}$)-*b*-^{XL}M(PI_{1424}-*b*-PFS_{63}) co-micelles did not elongate, thus verifying that CDSA was inhibited after cross-linking (fig. S8).

Next, we attempted to remove the central M(PFS_{60}-*b*-$PDMS_{660}$) micelle block from the ^{XL}M(PI_{1424}-*b*-PFS_{63})-*b*-M(PFS_{60}-*b*-$PDMS_{660}$)-*b*-^{XL}M(PI_{1424}-*b*-PFS_{63}) triblock co-micelles to release the ^{XL}M(PI_{1424}-*b*-PFS_{63}) daughter micelles designed to undergo unidirectional CDSA. We found that dispersions of the triblock co-micelles in a decane:toluene (3:5 by volume) solution resulted in the selective dissolution of the central M(PFS_{60}-*b*-$PDMS_{660}$) micelle block, leaving short ^{XL}M(PI_{1424}-*b*-PFS_{63}) daughter micelles

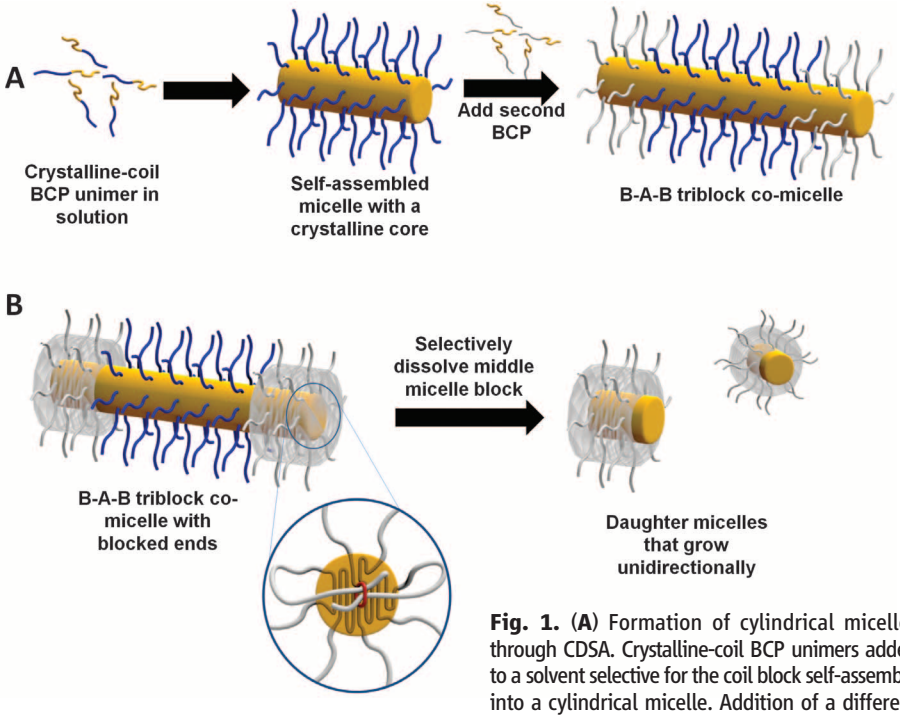

Fig. 1. (**A**) Formation of cylindrical micelles through CDSA. Crystalline-coil BCP unimers added to a solvent selective for the coil block self-assemble into a cylindrical micelle. Addition of a different crystalline-coil BCP unimer results in the lengthening of the previously formed micelle. (**B**) Proposed formation of non-centrosymmetric elongating cylindrical micelles. First, the core ends of a B-A-B micelle are obscured, preventing CDSA in both directions. Next, the middle micelle A block is selectively dissolved to create two daughter micelles, each with a blocked and a fully CDSA-active micelle core end.

with a length of 130 nm (PDI = 1.07) (Fig. 3C and figs. S9 and S10A). Upon removal of the toluene from the solution through selective evaporation, the dissolved PFS_{60}-*b*-$PDMS_{660}$ unimers grew onto only one side of the $^{XL}M(PI_{1424}$-*b*-$PFS_{63})$ daughter micelles (Fig. 3D and fig. S11), presumably off the end that was originally bound to the M(PFS_{60}-*b*-$PDMS_{660}$) domain, and thus formed non-centrosymmetric $^{XL}M(PI_{1424}$-*b*-$PFS_{63})$-*b*-M(PFS_{60}-*b*-$PDMS_{660}$) A-B diblock co-micelles with an average contour length of 220 nm (PDI = 1.04) (fig. S10B). The non-centrosymmetric A-B block co-micelles were also found to be active in further CDSA. For example, the addition of further PFS_{60}-*b*-$PDMS_{660}$ unimer resulted in the unidirectional elongation of the cylindrical A-B diblock co-micelles via CDSA (Fig. 3, E and F).

A key motivation behind the development of non-centrosymmetric nanoparticles is their use in the creation of complex objects via hierarchical self-assembly. By analogy with the behavior of surfactants and amphiphilic BCPs in selective solvents, we envisioned that non-centrosymmetric amphiphilic block co-micelles would also self-assemble into larger structures (Fig. 4A). Although CDSA has been shown to operate for crystalline-coil BCPs with either nonpolar (*19*) or polar coil blocks (*33*), amphiphilic block co-micelles containing both polar and nonpolar corona regions within the same micelle have not been described. However, we found that we were able to bidirectionally grow PFS_{64}-*b*-$P2VP_{837}$ [P2VP is poly(2-vinylpyridine)] micelle blocks off preformed M(PFS_{60}-*b*-$PDMS_{660}$) micelles via CDSA in a solvent mixture of iPrOH:decane (3:1 by volume, where iPr is isopropyl) at 45°C (fig. S12). Next, we set out to make non-centrosymmetric amphiphilic A-B-C $^{XL}M(PI_{1424}$-*b*-$PFS_{63})$-*b*-M(PFS_{60}-*b*-$PDMS_{660}$)-*b*-M(PFS_{64}-*b*-$P2VP_{837}$) triblock co-micelles by growing PFS_{64}-*b*-$P2VP_{837}$ (the polar component) off of the nonpolar $^{XL}M(PI_{1424}$-*b*-$PFS_{63})$-*b*-M(PFS_{60}-*b*-$PDMS_{660}$) A-B micelles. PFS_{64}-*b*-$P2VP_{837}$ unimer was added to a suspension of $^{XL}M(PI_{1424}$-*b*-$PFS_{63})$-*b*-M(PFS_{60}-*b*-$PDMS_{660}$) A-B micelles in iPrOH:decane (3:1 by volume) at 45°C and was allowed to age for 4 hours, during which time the solution became turbid. Transmission electron microscopy (TEM) micrographs of a drop-cast sample of the solution showed the

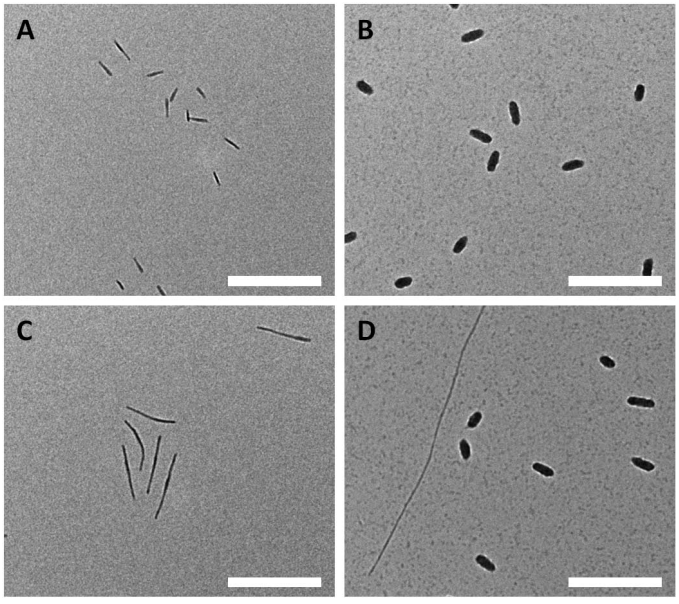

Fig. 2. (**A**) TEM micrograph of cylindrical M(PI_{1424}-*b*-PFS_{63}) micelles with an average contour length of 121 nm. (**B**) TEM micrograph of cross-linked cylindrical $^{XL}M(PI_{1424}$-*b*-$PFS_{63})$ micelles. The cross-linked $^{XL}M(PI_{1424}$-*b*-$PFS_{63})$ micelles appear darker in the TEM micrograph because of binding of residual platinum catalyst from the cross-linking procedure and contraction of the corona (*31*). (**C**) The addition of PFS_{60}-*b*-$PDMS_{660}$ unimers to a solution of non–cross-linked M(PI_{1424}-*b*-PFS_{63}) micelles resulted in an increase in the average micelle contour length from 121 to 275 nm because of the incorporation of PFS_{60}-*b*-$PDMS_{660}$ unimers via CDSA. (**D**) Upon addition of PFS_{60}-*b*-$PDMS_{660}$ unimer to cross-linked $^{XL}M(PI_{1424}$-*b*-$PFS_{63})$ micelles, the overwhelming majority (98%) of the cross-linked $^{XL}M(PI_{1424}$-*b*-$PFS_{63})$ micelles were resistant to the incorporation of PFS_{60}-*b*-$PDMS_{660}$ unimer and appeared inactive to CDSA. A long, self-nucleated M(PFS_{60}-*b*-$PDMS_{660}$) homomicelle is visible in the TEM micrograph. PDMS and non–cross-linked PI corona regions are not visible in TEM micrographs because of insufficient electron density contrast. Scale bars 500 nm.

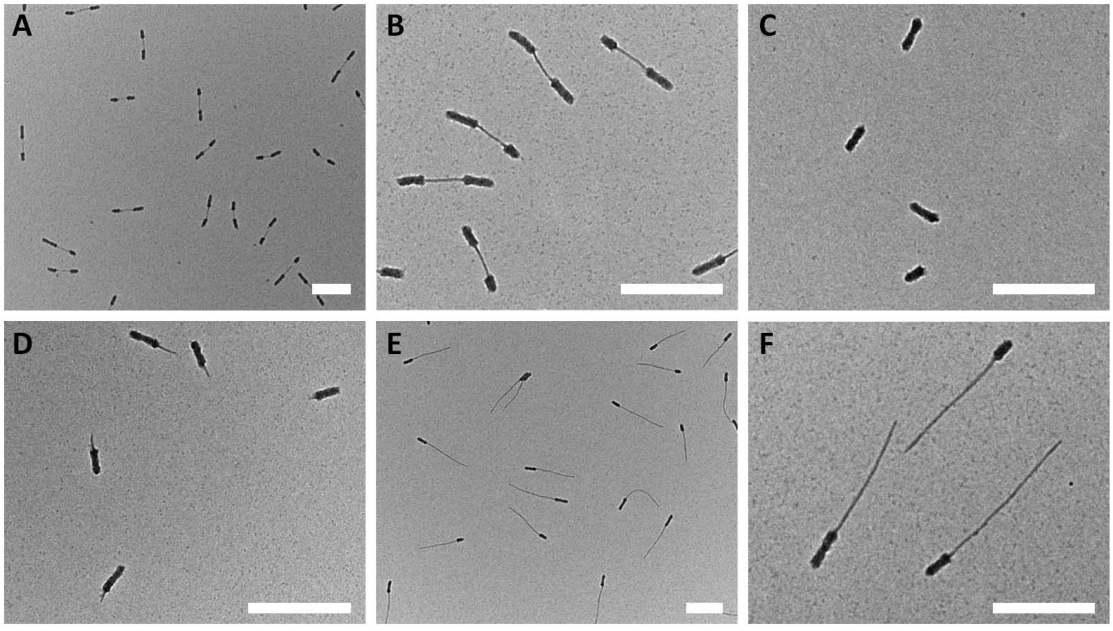

Fig. 3. (**A** and **B**) TEM micrographs of B-A-B $^{XL}M(PI_{1424}$-*b*-$PFS_{63})$-*b*-M(PFS_{60}-*b*-$PDMS_{660}$)-*b*-$^{XL}M(PI_{1424}$-*b*-$PFS_{63})$ triblock co-micelles, where the PI corona has been cross-linked. (**C**) TEM micrograph of $^{XL}M(PI_{1424}$-*b*-$PFS_{63})$ micelles formed from the dispersion of B-A-B $^{XL}M(PI_{1424}$-*b*-$PFS_{63})$-*b*-M(PFS_{60}-*b*-$PDMS_{660}$)-*b*-$^{XL}M(PI_{1424}$-*b*-$PFS_{63})$ triblock co-micelles in a decane:toluene (3:5 by volume) solution. In the presence of toluene, a good solvent for PFS, PDMS, and PI, the central PFS_{60}-*b*-$PDMS_{660}$ block of the triblock co-micelles dissolved; however, because of the cross-linking of the PI corona, the micelle blocks of $^{XL}M(PI_{1424}$-*b*-$PFS_{63})$ remained assembled in solution. (**D**) A-B $^{XL}M(PI_{1424}$-*b*-$PFS_{63})$-*b*-M(PFS_{60}-*b*-$PDMS_{660}$) diblock co-micelles formed after the removal of toluene from the toluene:decane solution. (**E** and **F**) Addition of more PFS_{60}-*b*-$PDMS_{660}$ unimer to the micelles results in unidirectional CDSA. PDMS corona regions are not visible in TEM micrographs because of insufficient electron density contrast. Scale bars, 500 nm.

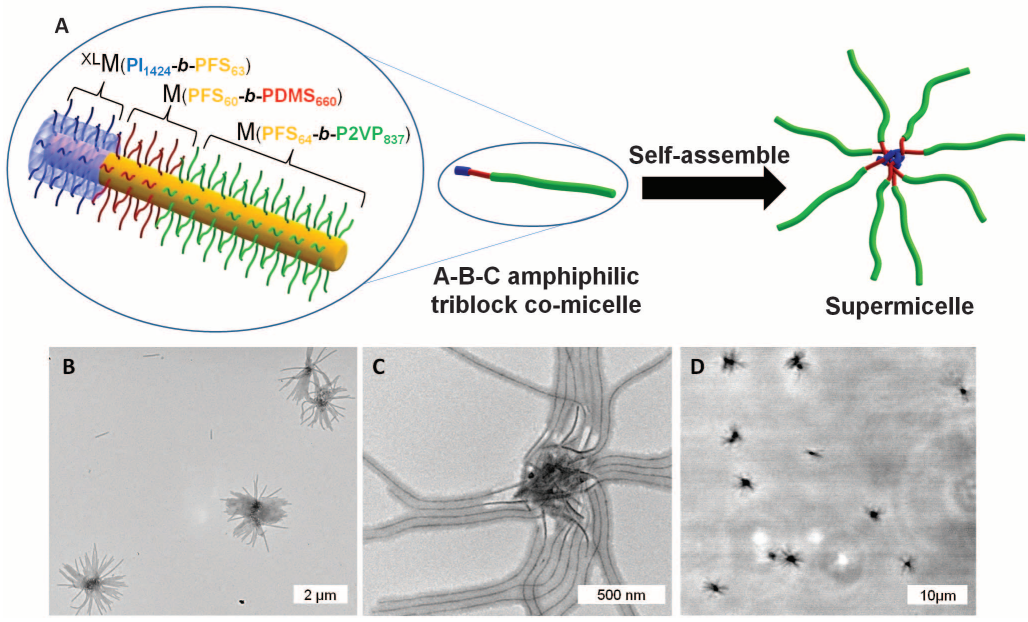

Fig. 4. (**A**) Schematic representation of an amphiphilic ^{XL}M(PI$_{1424}$-*b*-PFS$_{63}$)-*b*-M(PFS$_{60}$-*b*-PDMS$_{660}$)-*b*-M(PFS$_{64}$-*b*-P2VP$_{837}$) triblock co-micelle and its self-assembly into a supermicelle. (**B**) Low-magnification TEM micrograph of a cluster of supermicelles drop cast from iPrOH:decane (3:1 by volume). (**C**) Higher-magnification TEM micrograph of a supermicelle showing the core, composed of the cross-linked ^{XL}M(PI$_{1424}$-*b*-PFS$_{63}$), and a corona of M(PFS$_{64}$-*b*-P2VP$_{837}$) micelle blocks. The M(PFS$_{60}$-*b*-PDMS$_{660}$) blocks act as linkers between the supermicellular core and corona. PDMS corona regions are not visible in TEM micrographs because of insufficient electron density contrast. (**D**) Optical micrograph of the supermicelles suspended in iPrOH:decane (3:1 by volume).

formation of large starlike structures (~ 3 μm in diameter), which were aggregates of cylindrical micelles (Fig. 4B). On closer inspection, each individual co-micelle had a profile consistent with the target non-centrosymmetric amphiphilic ^{XL}M(PI$_{1424}$-*b*-PFS$_{63}$)-*b*-M(PFS$_{60}$-*b*-PDMS$_{660}$)-*b*-M(PFS$_{64}$-*b*-P2VP$_{837}$) (Fig. 4C) triblock co-micelle. As expected on the basis of the behavior of other amphiphilic systems of different sizes, the A-B-C amphiphilic block co-micelles assembled into star-shaped supermicelles. The "core" of the supermicelle was composed primarily of the ^{XL}M(PI$_{1424}$-*b*-PFS$_{63}$) block of the A-B-C triblock co-micelles, the "corona" was formed from the M(PFS$_{64}$-*b*-P2VP$_{837}$) block, and the M(PFS$_{60}$-*b*-PDMS$_{660}$) block acted as a linker between the core and corona. Given that the diameter of each of the supermicelles was ~3 μm in TEM micrographs, the supermicelles were also observed in optical microscope micrographs of the solution (Fig. 4D). Additionally, the supermicelles were found to be colloidally stable at room temperature over periods of months without flocculation.

We have demonstrated a previously unknown and versatile solution self-assembly approach to the controlled formation of non-centrosymmetric colloidally stable core-shell nanoparticles with shape anisotropy from BCPs. We have shown that short cylindrical micelles that undergo unidirectional CDSA can be prepared by selectively preventing growth at one end of a micelle through corona cross-linking. The resulting structures can be readily used as seeds to access non-centrosymmetric cylindrical block co-micelle architectures. The methodology was used to create amphiphilic A-B-C cylindrical block co-micelles that self-assembled into hierarchical supermicelles. Although the methodology described here was based on PFS-containing BCPs, it should also be applicable to the emerging group of other crystalline-coil BCPs that undergo CDSA. This will allow access to a wide variety of well-defined non-centrosymmetric architectures with control of segment length and segment composition. Of particular interest would be the application of this approach to conjugated polymer systems with different band gaps (*22*, *28*), with the goal of creating heterojunctions via solution self-assembly.

References and Notes

1. S. C. Glotzer, M. J. Solomon, *Nat. Mater.* **6**, 557 (2007).
2. S. Park, J. H. Lim, S. W. Chung, C. A. Mirkin, *Science* **303**, 348 (2004).
3. Q. Chen *et al.*, *Science* **331**, 199 (2011).
4. J. Howard, A. A. Hyman, *Nature* **422**, 753 (2003).
5. L. Zhang, A. Eisenberg, *Science* **268**, 1728 (1995).
6. H. Cui, Z. Chen, S. Zhong, K. L. Wooley, D. J. Pochan, *Science* **317**, 647 (2007).
7. Z. Li, E. Kesselman, Y. Talmon, M. A. Hillmyer, T. P. Lodge, *Science* **306**, 98 (2004).
8. D. A. Christian *et al.*, *Nat. Mater.* **8**, 843 (2009).
9. S. Jain, F. S. Bates, *Science* **300**, 460 (2003).
10. A. Walther, A. H. E. Müller, *Soft Matter* **4**, 663 (2008).
11. A. Walther *et al.*, *J. Am. Chem. Soc.* **131**, 4720 (2009).
12. J. Dupont, G. Liu, *Soft Matter* **6**, 3654 (2010).
13. A. Walther, X. André, M. Drechsler, V. Abetz, A. H. E. Müller, *J. Am. Chem. Soc.* **129**, 6187 (2007).
14. A. Walther, M. Drechsler, A. H. E. Müller, *Soft Matter* **5**, 385 (2009).
15. I. K. Voets *et al.*, *Angew. Chem. Int. Ed.* **45**, 6673 (2006).
16. L. Cheng, G. Zhang, L. Zhu, D. Chen, M. Jiang, *Angew. Chem. Int. Ed.* **47**, 10171 (2008).
17. D. J. Pochan *et al.*, *Soft Matter* **7**, 2500 (2011).
18. Y. Xia, B. D. Olsen, J. A. Kornfield, R. H. Grubbs, *J. Am. Chem. Soc.* **131**, 18525 (2009).
19. X. S. Wang *et al.*, *Science* **317**, 644 (2007).
20. T. Gädt, N. S. Ieong, G. Cambridge, M. A. Winnik, I. Manners, *Nat. Mater.* **8**, 144 (2009).
21. J. B. Gilroy *et al.*, *Nat. Chem.* **2**, 566 (2010).
22. S. K. Patra *et al.*, *J. Am. Chem. Soc.* **133**, 8842 (2011).
23. E. Lee *et al.*, *J. Am. Chem. Soc.* **133**, 10390 (2011).
24. N. Petzetakis, A. P. Dove, R. K. O'Reilly, *Chem. Sci.* **2**, 955 (2011).
25. J. Schmelz, M. Karg, T. Hellweg, H. Schmalz, *ACS Nano* **5**, 9523 (2011).
26. M. Lazzari, D. Scalarone, C. Vazquez-Vazquez, M. A. López-Quintela, *Macromol. Rapid Commun.* **29**, 352 (2008).
27. Z.-X. Du, J.-T. Xu, Z.-Q. Fan, *Macromolecules* **40**, 7633 (2007).
28. W. Zhang *et al.*, *Science* **334**, 340 (2011).
29. R. K. O'Reilly, C. J. Hawker, K. L. Wooley, *Chem. Soc. Rev.* **35**, 1068 (2006).
30. X. S. Wang *et al.*, *J. Am. Chem. Soc.* **129**, 5630 (2007).
31. P. A. Rupar, G. Cambridge, M. A. Winnik, I. Manners, *J. Am. Chem. Soc.* **133**, 16947 (2011).
32. J. Qian *et al.*, *Angew. Chem. Int. Ed.* **50**, 1622 (2011).
33. H. Wang, M. A. Winnik, I. Manners, *Macromolecules* **40**, 3784 (2007).

Acknowledgments: P.A.R. is grateful to the Natural Science and Engineering Research Council (NSERC) of Canada for a postdoctoral fellowship and the European Union (EU) for a Marie Curie fellowship. L.C. thanks the EU and Engineering and Physical Sciences Research Council for support. I.M. thanks the EU for a Marie Curie Chair, a Reintegration Grant, and a European Research Council Advanced Investigator Grant and the Royal Society for a Wolfson Research Merit Award. M.A.W. thanks the NSERC of Canada for financial support. The authors also thank T. Gädt for synthesizing PFS$_{28}$-*b*-PDMS$_{560}$ and PFS$_{64}$-*b*-P2VP$_{837}$.

Supplementary Materials

www.sciencemag.org/cgi/content/full/337/6094/559/DC1
Materials and Methods
Figs. S1 to S12
Tables S1
References (*34*–*36*)

28 February 2012; accepted 25 May 2012
10.1126/science.1221206